Self-consistent cluster calculations with correct embedding for 3d, 4d, and some sp impurities in copper

P. J. Braspenning

Natuurkundig Laboratorium der Vrije Universiteit van Amsterdam, 1018-XE Amsterdam, The Netherlands

R. Zeller

Institut für Festkörperforschung, Kernforschungsanlage Jülich, D-5170 Jülich, West Germany

A. Lodder

Natuurkundig Laboratorium der Vrije Universiteit van Amsterdam, 1018-XE Amsterdam, The Netherlands

P. H. Dederichs

Institut für Festkörperforschung, Kernforschungsanlage Jülich, D-5170 Jülich, West Germany

Self-consistent calculations are presented for the electronic structure of 3d, 4d, and some sp impurities in Cu. The calculations are based on density-functional theory in the local-spin-density approximation and on the Korringa-Kohn-Rostoker Green's-function method. The muffin-tin potentials of the impurity *and* of the neighboring atoms are calculated self-consistently. The use of the proper host Green's functions guarantees the correct embedding of this cluster of 13 muffin-tin potentials in the ideal Cu host. One shell of perturbed neighbor potentials is sufficient for a good description of the electronic properties. While the results considerably improve the previous single-site calculations, they nevertheless confirm for most impurities the qualitative results obtained in these calculations. Charge-transfer effects are most pronounced for some 4d impurities and the vacancy. The magnetic moments of the 3d impurities are only slightly changed compared to the single-site calculations.

I. INTRODUCTION

In the last ten years dramatic progress has been achieved in understanding the electronic structure of ideal crystals, which is essentially due to the development of density-functional theory and linearized band-structure methods. For inhomogeneous problems such as point defects or surfaces, similar progress is to be expected as soon as methods analogous to and as efficient as the present band-structure methods are developed for these systems. Whereas for concentrated alloys the development of the Korringa-Kohn-Rostoker (KKR) version of the coherent-potential approximation has been an important step in this direction, for dilute alloys the Green's-function method proposed and applied by different groups has shown considerable potential.

The advantage of the Green's-function method compared to other methods such as cluster calculations is that due to the introduction of the host Green's function, the embedding of the defect in the ideal crystal is described correctly. All band-structure effects are taken into account. Furthermore, only the perturbed potential $\Delta V(\vec{r})$ enters as a perturbation, contrary to usual cluster or super-cell calculations, where the total potential had to be always considered. This has some important practical advantages. The change ΔV of the potential is strongly localized near the defect, so that very often only a perturbation in the impurity cell is sufficient. We will discuss this point in detail in this paper. Furthermore, the self-consistency process is divided into two natural steps: first the ideal-crystal problem leading to the self-consistent Green's function $\tilde{G}$ and second the defect problem where all defects and all self-consistency cycles can be calculated with the same $\tilde{G}$.

The Green's-function method was originally proposed by Koster and Slater.[1] However, only recently have self-consistent calculations based on a linear combination of atomic orbitals (LCAO) expansion been performed for defects in semiconductors.[2-5] For metals a Green's-function method based on the KKR band-structure scheme has been proposed by Dupree,[6] Beeby,[7] and others. Detailed calculations along this line have been performed by Terakura[8] and more recently by Katajama-Yoshida et al.[9] We have improved this method by doing self-consistent calculations within the density-functional scheme.[10] Detailed calculations for magnetic impurities in Cu (Refs. 11 and 12), nonmagnetic impurities in Cu (Ref. 13), impurities in Al (Ref. 14), 3d and 4d impurities in Mo and Nb (Ref. 15), as well as d impurities in Ni (Ref. 16) have been presented. These calculations are all based on a muffin-tin assumption for the atomic potentials. Moreover and more essentially, only the impurity muffin-tin potential was allowed to be perturbed and calculated self-consistently; a possible perturbation of the neighboring host potentials was neglected.

A variant of the KKR Green's-function method based

on an expansion in linear muffin-tin orbitals (LMTO) has been recently given by Koenig and Daniel.[17] Calculations for sp impurities[18] and 3d impurities[19] in Fe have been performed by this group, which are also based on the assumption of a single perturbed muffin-tin potential. Recently Klein and Pickett[20] have published calculations for H in transition metals. A quite different Green's-function approach has been recently given by Inglesfield.[21] Here the embedding is described rigorously by an energy-dependent complex surface potential surrounding a given cluster.

Despite the fact that the above calculations have been quite successful in explaining trends and experimental data, in general the assumption of a single perturbed potential seems to be a rather restrictive approximation because it limits a possible response of the host atoms. We will also demonstrate in this paper that clusters of perturbed potentials can be treated with the Green's-function scheme, i.e., perturbed potentials at neighboring sites of the defect can also be included and calculated self-consistently. Since this is a much more involved problem than the single-site perturbation, we have developed special methods in order to reduce the necessary computing time. For instance, by using the method of complex-energy integration[22] the Schrödinger equation need only be solved for a small number (20—50) of complex energies rather than about 1000 real energies. We found it necessary to use group theory in our calculations, and we have used improved iteration schemes in order to reduce the number of self-consistency iterations. These technical points are described in Sec. II.

In the following sections we present detailed calculations for impurities in Cu. Section III deals with 4d and nonmagnetic 3d impurities, Sec. IV with magnetic 3d impurities, and Sec. V with some sp impurities such as H, He (both in a vacancy), Mg, Si, and Ag. A communication about a calculation for the vacancy in Cu has already been published elsewhere.[23] An important result of these calculations is that for most impurities the qualitative results obtained by using a single perturbed potential are confirmed. The effect of the perturbed neighboring potentials is, in general, small but quantitatively nevertheless important if such details as charge transfer, induced host magnetization, or Friedel oscillations are described. There are also, however, exceptional cases like Co in Cu or the Cu vacancy where the inclusion of the perturbed host potentials changes the situation qualitatively. Recently, the LMTO Green's-function technique has been studied in detail by Gunnarsson et al.,[24] who also presented with this method test calculations that include potential perturbations at neighboring sites.

II. SOME TECHNICAL POINTS CONCERNING THE KKR GREEN'S-FUNCTION METHOD

In this section we summarize some technical problems related to the application of the KKR Green's-function method.[11] For a lattice of muffin-tin potentials $v_n(\vec{r} - \vec{R}^n)$ centered at positions $\vec{R}^n$, the Green's function can be expanded in each cell n, n' into eigensolutions of the local muffin-tin potentials v_n and $v_{n'}$.

$$G(\vec{r} + \vec{R}^n, \vec{r}' + \vec{R}^{n'}, E)$$

$$= -i\delta_{nn'}\sqrt{E} \sum_L Y_L(\vec{r}) R_l^n(r_<, E) H_l^n(r_>, E) Y_L(\vec{r}')$$

$$+ \sum_{L,L'} Y_L(\vec{r}) R_l^n(r, E) G_{LL'}^{nn'}(E) R_{l'}^{n'}(r', E) Y_{L'}(\vec{r}') .$$

(1)

Here Rydberg units $(e = 1, \hbar^2/2m = 1)$ have been used. The vectors $\vec{r}, \vec{r}'$ are restricted to the Wigner-Seitz cell, and $r_<$ and $r_>$ are the smaller and larger of $r = |\vec{r}|$ and $r' = |\vec{r}'|$. Y_L is a real spherical harmonic and $R_l^n(r, E)$ is the regular solution of the radial Schrödinger equation for the potential $v_n(r)$ and the energy E. Furthermore, L stands for $L = (l, m)$. Outside the muffin-tin radius, $H_l^n(r, E)$ agrees with the spherical Hankel function $h_l = j_l + in_l$, and $R_l^n(r, E)$ is given by a combination of spherical Hankel and Bessel functions

$$H_l^n(r, E) = h_l(r\sqrt{E}) ,$$

(2)

$$R_l^n(r, E) = j_l(r\sqrt{E}) - i\sqrt{E} \, t_l^n(E) h_l(r\sqrt{E}) ,$$

ior $r > R_{MT}$, where $t_l^n(E)$ denotes the usual on-shell t matrix for the potential v_n.

The first term in Eq. (1) represents the solution for the single muffin-tin potential v_n in free space. Of central importance is the so-called structural Green's-function matrix $G_{LL'}^{nn'}(E)$, which contains all the information about the multiple scattering between the muffin-tin potentials of the specific ensemble. It can be related by an algebraic Dyson equation to the structural Green's function $\widetilde{G}_{LL'}^{nn'}(E)$ of the ideal crystal:

$$G_{LL'}^{nn'}(E) = \widetilde{G}_{LL'}^{nn'}(E) + \sum_{L'',n''} \widetilde{G}_{LL''}^{nn''}(E) \Delta t_{l''}^{n''}(E) G_{L''L'}^{n''n'}(E) .$$

(3)

Note that here the deviation $\Delta t_l^n = t_l^n - \tilde{t}_l$ of the t matrix t_l^n from the ideal-crystal value $\tilde{t}_l$ enters as perturbation.

A. Determination of the structural host Green's function

One major problem of the KKR Green's-function method is the determination of the structural Green's function $\widetilde{G}_{LL'}^{nn'}(E)$ of the host. The imaginary part can be evaluated by a numerical Brillouin-zone integration, similar to density of states integrals. The real part can, in principle, be obtained from the imaginary part by a Kramers-Kronig integration:

$$\alpha_{ll'}(E) \text{Re} \widetilde{G}_{LL'}^{(m-m')}(E) = \frac{1}{\pi} \int_{-\infty}^{+\infty} dE' \text{P} \left[\frac{1}{E - E'} \right] \alpha_{ll'}(E')$$

$$\times \text{Im} \widetilde{G}_{LL'}^{(m-m')}(E') . \quad (4)$$

For convenience we have integrated out the radial dependence leading to normalization coefficients $\alpha_{ll'}(E)$.

In actual calculations the E' integration in (4) requires the knowledge of the band structure up to infinite energies, which is impossible to obtain. For the diagonal part

$m = m'$ one can choose a cutoff energy E_c.[10] This means that above E_c one replaces $\widetilde{G}(\vec{r} + \vec{R}^{\,m}, \vec{r}\,' + \vec{R}^{\,m}; E')$ by the solutions $\widetilde{G}_1(r + R^{\,m}, \vec{r}\,' + \vec{R}^{\,m}; E')$ for a single muffin-tin potential. For the nondiagonal terms $m \neq m'$ a simple cutoff in Eq. (4) is not satisfactory. Instead we replace $\widetilde{G}(\vec{r} + \vec{R}^{\,m}, \vec{r}\,' + R^{\,m'}; E')$ for $E' > E_c$ by the solution $\widetilde{G}_2(\vec{r} + \vec{R}^{\,m}, \vec{r}\,' + \vec{R}^{\,m'}; E')$ for two muffin-tin potentials in free space, located at $\vec{R}^{\,m}$ and $\vec{R}^{\,m'}$. Then we obtain from Eq. (4) for $m \neq m'$

$$\alpha_{ll'}(E)\,\mathrm{Re}[\,\widetilde{G}_{\,LL'}^{\,(m-m')}(E) - \widetilde{G}_2{}_{LL'}^{\,(m-m')}(E)]$$

$$= \frac{1}{\pi} \int_{-\infty}^{E_c} dE'\, \mathrm{P}\left[\frac{1}{E - E'}\right] \alpha_{ll'}(E')$$

$$\times \mathrm{Im}[\,\widetilde{G}_{LL'}^{\,(m-m')}(E') - \widetilde{G}_2{}_{LL'}^{\,(m-m')}(E')]\,, \quad (5)$$

since also $\widetilde{G}_2$ obeys a Kramers-Kronig relation. The sensitivity of the results to the choice of E_c is discussed later. It should be pointed out that in other Green's-function methods based on LCAO or LMTO expansions, this problem of integrating over infinite energies does not ostensibly occur. Here a corresponding cutoff assumption is made just at the beginning by taking only a finite basis set into account.

B. Solution of the Dyson equation

The structural Green's function of the imperfect crystal is obtained from that of the host crystal by solving the Dyson equation (3). In general, this requires the inversion of the matrix

$$\delta_{nn'}\delta_{LL'} - \widetilde{G}_{LL'}^{\,nn'}(E)\Delta t_{l'}^{n'}(E)\,. \quad (6)$$

The rank of this matrix is determined by the number of perturbed potentials and the number of nonzero elements $\Delta t_l^n(E)$, respectively. When only the impurity site is considered as perturbed, one must invert a matrix of rank 9×9 for $l \leq 2$. For cubic symmetry the impurity structural matrix $G_{LL'}^{00}$ is diagonal in angular momentum, and the Dyson's equation reduces further to four scalar equations ($s, p, d\ t_{2g}$ and $d\ e_g$ representations) that are easily solved. However, in the present cluster calculation, for an impurity in a fcc material with perturbed first neighbors and for $l \leq 2$, matrices of rank 117×117 must be inverted for each energy since 13 atoms and nine angular momenta are involved ($117 = 9 \times 13$). In addition to requiring self-consistency, this clearly is an enormous numerical effort, especially since the entire energy range must be considered.

Group theory can be very useful here. It allows for a quasidiagonalization of the matrix to be inverted, such that, in this case (fcc for $l \leq 2$), the largest submatrix has a rank of 9×9. The total amount of submatrices equals 10, corresponding to the different irreducible representations of the point group. The quasidiagonalization is accomplished by the unitary (orthogonal) matrix S such that the submatrices are given by

$$G_{\mu(l),\nu(l')}^{\lambda\alpha} = \sum_{\substack{n \in s \\ n' \in s' \\ m,m'}} S_{nlm,\mu}^{\lambda\alpha} G_{lm,l'm'}^{nn'} S_{n'l'm',\nu}^{\lambda\alpha}\,. \quad (7)$$

This well-known symmetrization procedure requires that at both sides of the structure matrix the elements $S_{nlm,\mu}^{\lambda\alpha}$ are needed for all sites n in shell s and all m values belonging to the given value of the angular momentum l. The index μ denotes the basis function belonging to a particular column α of the representation λ. It is a compound index counting the particular combinations (lns) of the angular momentum l, the shell s, and the number of linear independent combinations n of a certain value of the quartet ($\lambda \alpha l s$). The elements of the symmetrized matrix do not depend on the specific column α of the irreducible representation λ, which is a well-known group-theoretical result. The maximum number of columns is 3, appearing for only 4 of the 10 representations. This (two-sided) symmetrization procedure leads to a reduction factor of 6 for the computer time needed for the inversion of the matrix (i.e., for the inversion of all the different submatrices).

However, as noted by Rijsenbrij and Lodder[25] and Ries and Winter,[26] the use of one-sided symmetrization leads to a larger reduction of the computer time, because then the summation over all sites in a particular shell is replaced by the summation over the columns at *one* side of the matrix, which must be symmetrized. Thus the following also holds:

$$G_{\mu(l),\nu(l')}^{\lambda\alpha} = \frac{N_{s'}}{d_\lambda} \sum_{\substack{n \in s \\ \gamma,m,m'}} S_{nlm,\mu}^{\lambda\gamma} G_{lm,l'm'}^{nn_0'} S_{n_0'l'm',\nu}^{\lambda\gamma}\,, \quad (8)$$

where N_s is the number of atoms in shell s and α is merely a specific column in the set $\gamma = 1, 2, \ldots, d_\lambda$. The method of Ries and Winter uses the site index n_0' in shell s' fixed for all basis functions, although of course the choice of n_0' depends on the shell index used.

The fact that a summation of the atoms is equivalent to a summation over their counterparts allows for an additional reduction factor of 4. Lastly, the structural matrix of the perfect crystal needs to be symmetrized only once for each energy and can be stored on tape instead of calculating it again in each iteration cycle. This gives an additional reduction factor of about 3 so that the use of group theory is altogether very valuable, because a large factor of about 70 can be gained in the very time-consuming step (95%) of inverting huge matrices at a rather large amount of energy points.

C. Energy integration for obtaining charge densities

The charge density $\rho(r)$ is obtained by an energy integration

$$\rho(r) = -\frac{2}{\pi} \int_{-\infty}^{E_F} dE\, \mathrm{Im}\, G(\vec{r}, \vec{r}; E)\,. \quad (9)$$

Owing to the strong structure in the Green's function $G(E)$ induced by the d electrons, reliable charge densities can only be obtained by using about 400 energies for the charge density in the impurity cell, while the charge density in the neighboring cells requires even more than 1000

energy points. Thus the radial Schrödinger equations and the Dyson equation (3) would have to be solved in each iteration cycle for an enormous number of energies. A very elegant solution of this problem can be found by replacing the energy integral of the imaginary part of the Green's function by a contour integral in the complex-energy plane (Koenig[27] and Dreysse and Riedinger[28]):

$$\rho(\vec{r}) = \frac{i}{\pi} \oint dz \, G(\vec{r}, \vec{r}; z) \; . \tag{10}$$

The contour starts at $E_F - i\epsilon$ and ends at $E_F + i\epsilon$ ($\epsilon \to 0+$), including all branch cuts and poles of $G(z)$ on the real axis below E_F. The analytical property of $G(z)$ off the real axis prevents any strong structure along the contour and warrants a sufficiently smooth integrand, which can be integrated with only 20–40 complex-energy points instead of the enormous amount needed on the real axis. Details can be found elsewhere.[22,29] Thus the radial Schrödinger equation and the Dyson equation are only solved for a rather small number of complex energies, which does not only lead to a considerable saving of computer time but also to increased numerical accuracy.

D. Spin polarization and Lloyd's formula

The use of spin polarization requires an additional index for spin up ($\uparrow$) and spin down ($\downarrow$). That is, for each spin direction we have different potentials, phase shifts, Green's functions, etc., so that all equations (for instance, the Dyson equation) appear twofold. Furthermore, the densities (of charge and of states) are obtained separately for each spin direction by an energy integration or space integration. Then the local charge N_{loc} and local moment M_{loc} within the cell n are given by

$$M_{loc}^n = N_{loc,\uparrow}^n - N_{loc,\downarrow}^n$$

$$= \int_{-\infty}^{E_F} dE [N_{loc,\uparrow}^n(E) - N_{loc,\downarrow}^n(E)]$$

$$= \int_{V_n} d\vec{r} [\rho_\uparrow(\vec{r}) - \rho_\downarrow(\vec{r})] \tag{11}$$

$[N_{loc,\uparrow}^n(E)$ being the local density of states in the cell n for spin up and $\rho_\uparrow$ the corresponding local charge density] and

$$N_{loc}^n = N_{loc,\uparrow}^n + N_{loc,\downarrow}^n \; . \tag{12}$$

The total displaced charge is given by the change $\Delta N(E_F)$ of the integrated density of states at the Fermi energy, which can be calculated by Lloyd's formula (see below):

$$\Delta N(E_F) = \Delta N_\uparrow(E_F) + \Delta N_\downarrow(E_F) \; . \tag{13}$$

Analogously, the change of the total moment ΔM induced by the impurity is given by

$$\Delta M = \Delta N_\uparrow(E_F) - \Delta N_\downarrow(E_F) \; , \tag{14}$$

which is merely the total moment if the host is paramagnetic.

The integrated densities of states $\Delta N(E_F)$ can be calculated by Lehmann's adaptation of Lloyd's formula,[30,31] which for a cluster of perturbed potentials is slightly more complicated than that for a single perturbed potential:

$$\Delta N_\uparrow(E) = \frac{1}{\pi} \left[\sum_{n,L} \Delta \delta_{l\uparrow}^n(E) \right] - \frac{1}{\pi} \text{Im} \ln \det |1 - \widetilde{G} \, \Delta t_\uparrow| \; . \tag{15}$$

A more direct derivation has been recently given by one of us.[32] Here $\Delta \delta_{l\uparrow}^n = \delta_{l\uparrow}^n - \tilde{\delta}_l$ is the change of the phase shifts with respect to the host crystal. The determinant refers to the matrix of Eq. (6).

In Eq. (14) contributions due to polarization of all neighboring host atoms are included, whereas the cluster magnetic moment calculated as

$$M_{cl} = \sum_{n \text{ in cluster}} M_{loc}^n \tag{16}$$

contains only the polarization of the first neighbors.

Since only perturbed host potentials at the first shell around the impurity are allowed, the Friedel sum rule $\Delta N(E_F) = \Delta Z$ is not satisfied exactly in our calculation. Thus the deviation of $\Delta N(E_F)$ from the ideal value ΔZ gives an indication of the error involved and of the importance of including more perturbed shells.

E. Density-functional theory and improved iteration schemes

Our calculations are based on density-functional theory.[33] We use the local-density approximation of Hedin and Lundqvist[34] for the non-spin-polarized case and that of von Barth and Hedin[35] in the case of spin polarization. The necessary parameters in these forms were chosen to agree with those of Moruzzi et al.[36]. The host band structure of Cu has been generated from the self-consistent potentials given by these authors.

The Green's function of the impurity system, which determines the charge density in the different perturbed cluster cells, depends on the potentials $v_n(\vec{r})$, which themselves are related to the charge density. The self-consistency problem is therefore of the form $\rho(\vec{r}) = F\{\rho(\vec{r})\}$. A well-known solution consists of rewriting $\rho = (1-\alpha)\rho + \alpha F\{\rho\}$ and iterating towards self-consistency:

$$\rho_{n+1} = (1-\alpha)\rho_n + \alpha F\{\rho_n\} \; . \tag{17}$$

One can show that for a sufficiently small mixing factor, one always obtains a convergent process.[37] However, in impurity calculations we found this to be a serious problem. Especially, for d impurities with virtual bound states at the Fermi energy we had to choose α's as small as 10^{-2}, and consequently hundreds of iterations were necessary. Physically, this is due to the fact that a small change of the potential sweeps the virtual bound state through the Fermi energy, thereby drastically changing its population.

In order to accelerate the convergence we have recently studied improved iteration schemes.[37] In one scheme given by Anderson[38] the input charge density ρ_{n+1} for the iteration $n+1$ is constructed by using information from more than one previous iteration. One introduces a free parameter Θ_n and constructs linear combinations of ρ_n and ρ_{n-1}, $F\{\rho_n\}$ and $F\{\rho_{n-1}\}$ by

$$\rho_n^* = \rho_n + \Theta_n(\rho_{n-1} - \rho_n)$$

and   (18)

$$F_n^* = F\{\rho_n\} + \Theta_n(F\{\rho_{n-1}\} - F\{\rho_n\}) .$$

Θ_n is determined by minimizing the integral

$$\int d\vec{r} \mid \rho_n^*(\vec{r}) - F_n^*(\vec{r}) \mid^2$$

with respect to Θ_n. The input charge density for the next iteration is chosen (similar to the normal mixing scheme) as

$$\rho_{n+1} = (1 - \alpha^*)\rho_n^* + \alpha^* F_n^* ,$$

where α^* can usually be somewhat larger than the normal mixing factor α. In most cases the larger α^* and the optimization with respect to Θ_n lead to a better convergence, which sometimes is surprisingly fast. However, the convergence behavior at times can be quite irregular, so it is advantageous to return to the normal mixing scheme (17) for 10 or 20 iterations and then proceed with the improved scheme.

Our calculations rely on the muffin-tin approximation for the potentials. However, no muffin-tin approximation is made for the charge density, the full nonspherical components of which are considered. The intercell Coulombic potential is calculated by using a multipole expansion for the charge density. The potential is brought into muffin-tin form by spherically averaging inside the muffin-tin spheres and by using the constant host interstitial potential outside the spheres.

III. NONMAGNETIC 4d AND 3d IMPURITIES

The electronic structure of $4d$ impurities in Cu is not complicated owing to the occurrence of magnetism. We find all $4d$ impurities in Cu to be nonmagnetic; the Stoner criterion is far from being met.[13] Of the $3d$ impurities, only Sc, Ti, and Ni are nonmagnetic. The other $3d$ impurities V, Cr, Mn, Fe, and Co are magnetic and are discussed in the next section. A comparison of the $4d$ impurities with their chemically equivalent $3d$ counterparts should be especially interesting because the $4d$ impurities have a larger size and also a larger electronegativity than their $3d$ partners.

A. Local densities of states of the impurities and their nearest neighbors

Figure 1 gives the local density of states (LDOS) for the series Y, . . . , Pd of $4d$ impurities in Cu. Band-structure effects are seen to be very important. There is a rather large amount of structure in the Cu d-band region (from 1.6 to 5.3 eV below E_F), and a great quantity of intensity is distributed in this region, being more peaked at lower energies. Furthermore, the virtual bound states near the Fermi energy are rather broad at the beginning of the series and become increasingly sharper, until for Pd where we have an extremely sharp peak at the upper end of the Cu d band. Note that the virtual bound states are not Lorentzian but rather unsymmetric.

It is interesting to compare the present impurity-cluster

calculations (ICC) with the previous single-site calculation,[13] where only the impurity potential was calculated self-consistently. The present calculation yields an appreciably lower intensity in the lower d-band region, which is most dramatic for Cu(Pd). Here the peak at the bottom of the d band is substantially lowered, whereas the very small virtual bound state peak is increased.

As a representative example we will discuss Cu(Mo) in more detail. Figure 2(a) shows again the LDOS for Mo in Cu. The dashed line refers to the Mo LDOS obtained from the self-consistent impurity potential by calculating only the first term in Eq. (1), i.e., the Green's function for the single muffin-tin potential of the impurity in the muffin-tin zero-background potential ("no backscattering"). Physically, this essentially describes only the interaction of the Mo $4d$ electrons with the more or less free s and p electrons of Cu, leading to a rather broad virtual bound state centered at the upper d band of Cu. Since the interaction between the Mo $4d$ and the Cu $3d$ electrons is essentially switched off, we see that the hybridization between the Mo $4d$ and the Cu $3d$ electrons is very important: It shifts the virtual bound state to higher energies and at the same time leads to an additional intensity in the lower band region.

The LDOS of a Cu atom neighboring Mo is shown in Fig. 2(b) together with the unperturbed host density of states of Cu. On the neighboring site an appreciable part of the intensity is shifted to lower energies, while at the same time a small hump near the Fermi energy commemorates the virtual bound state at the Mo site.

The features seen in Figs. 2(a) and 2(b) can be understood by the formation of bonding and antibonding states between the Mo $4d$ and Cu $3d$ electrons. For a diatomic molecule with nondegenerate orbitals this is schematically illustrated in Fig. 3. Note that the Mo $4d$ level is higher than the Cu $3d$ level. A lower bonding level E_b and a higher antibonding level E_a are formed. Since E_a is closer to the Mo level and E_b is closer to the Cu level, the bonding wave function ψ_b has a larger amplitude for the Cu site, as is illustrated in Fig. 3(b). Therefore the hybridization can also be considered as an effective repulsion between the unhybridized levels.

In reality, the situation is more complicated than that in Figs. 3(a) and 3(b), since the d levels are degenerate and since there are 12 Cu neighbors instead of one; moreover, the 12 Cu neighbors are embedded in a Cu host environment. However, qualitatively the situation is still similar: The unhybridized Mo $4d$ levels, being broadened due to the interaction with the s electrons of the host [dashed curve in Fig. 2(a)] and the pure Cu levels on the neighboring site [dashed curve in Fig. 2(b)], hybridize and form bonding and antibonding states. Thus the new virtual bound state resembles the antibonding peak and is shifted to higher energies while being mostly concentrated on the Mo site. Furthermore, on the neighboring sites the strong shift of the intensity to lower energies is due to the formation of bonding orbitals, which are mostly centered at the neighboring sites. [Note that in order to calculate the change of the total density of states one must multiply the intensity changes seen in Fig. 2(b) for one neighbor by 12, the number of first neighbors, in order to compare them
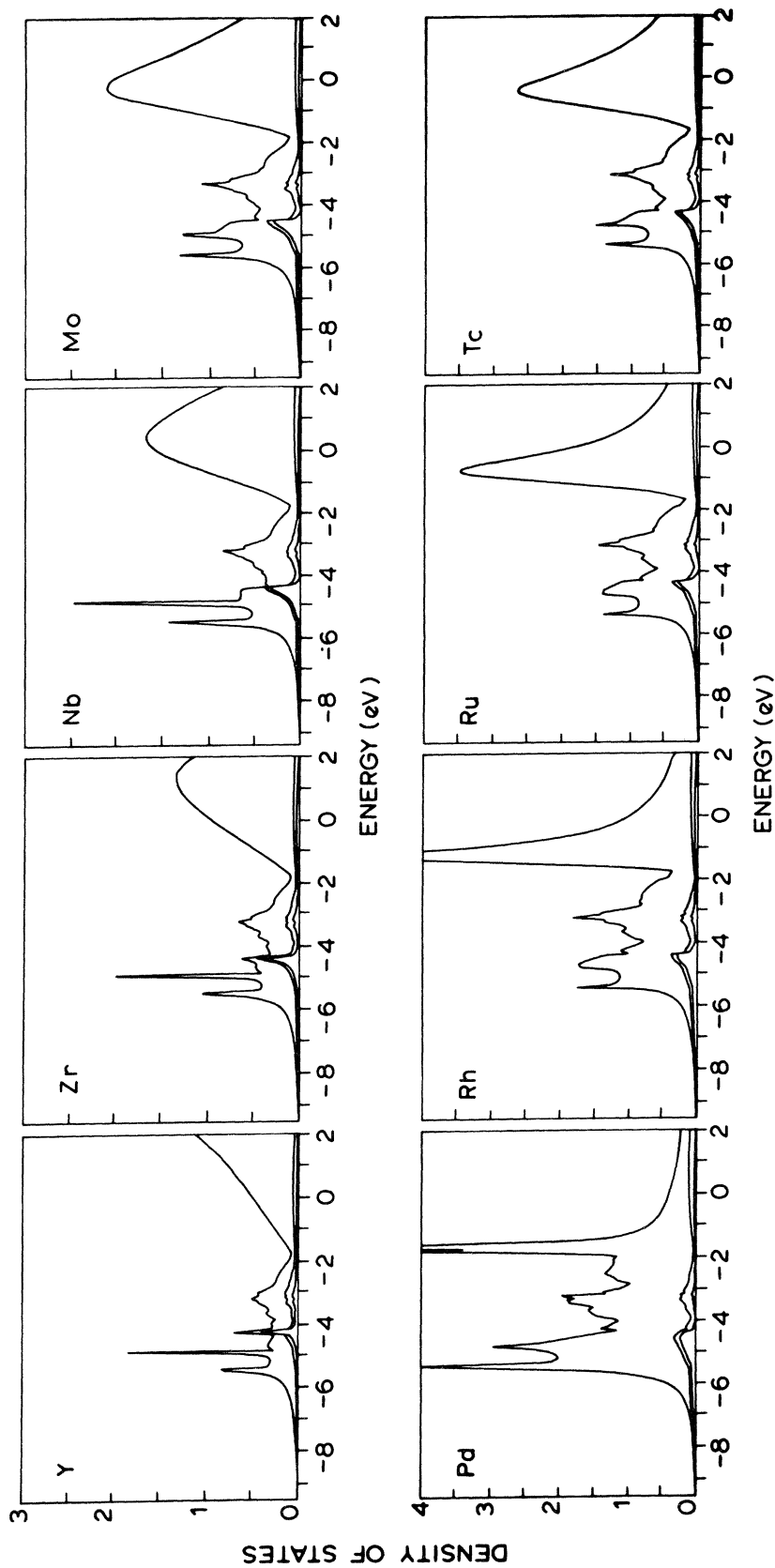
FIG. 1. LDOS in the impurity Wigner-Seitz cell for 4d impurities in Cu. The lower curve gives the s contribution, the second curve the sum of the s and p contributions, and the uppermost curve the total density of states as the sum of the s, p, and d contributions. Units: states/eV. Energy relative to Fermi energy.
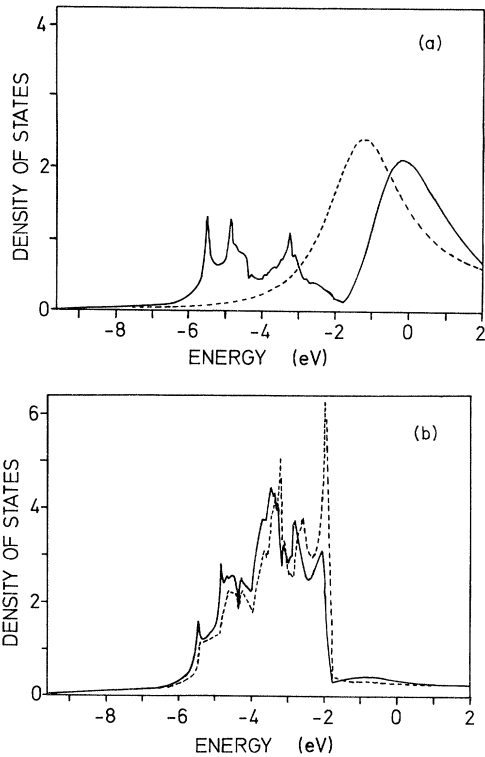
FIG. 2. (a) LDOS for Mo in Cu (solid line). The dotted curve refers to the solution for the single Mo muffin-tin potential in the constant muffin-tin zero-background potential (no "back-scattering"). (b) LDOS of a Cu atom neighboring Mo (solid line) and the unperturbed host density of states of Cu (dotted line).

with the "bonding" intensity within the d band on the Mo site.]

Figure 4 shows the LDOS on a neighboring site for Nb, Tc, and Rh, whereas Fig. 5 shows the corresponding change of the neighbor LDOS with respect to the host density of state for Zr, Mo, Rh, and Pd. Especially Fig. 5 shows clearly that the shift of the intensity to lower energies is a well-defined trend for the entire $4d$ series. It is more pronounced at the beginning of the series, which can be explained by the larger extent of the $4d$ wave functions
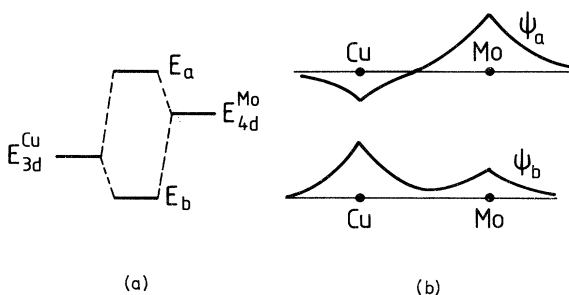
FIG. 3. (a) Schematic representation of the hybridization of the atomic Cu and Mo levels into bonding and antibonding energy levels E_b, E_a. (b) Schematic form of the bonding and antibonding wave functions at the Cu and Mo sites.
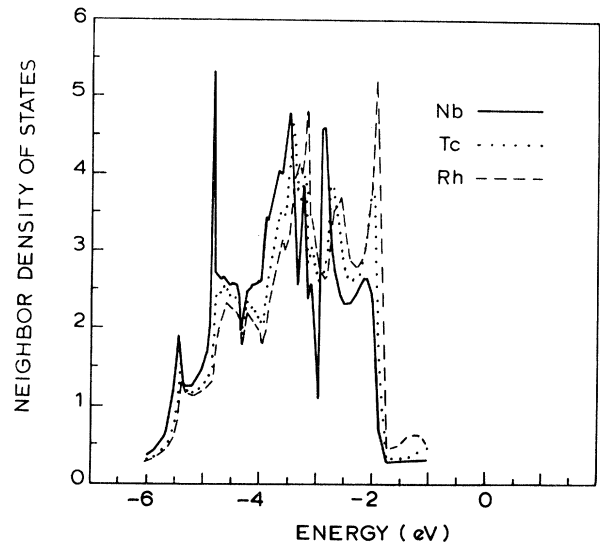

FIG. 4. LDOS in Cu-neighbor Wigner-Seitz cell of some elements from the $4d$ series. Only the behavior in the Cu d-band energy region and somewhat above it is shown.

(leading to a stronger overlap with the Cu d electrons) and by the larger splitting between the corresponding $4d$ level and the Cu level. For Pd at the end of the $4d$ series we see a peak at the upper band edge, resembling the very narrow virtual bound state and two peaks at the lower end of the band. Essentially the same structure is seen at the impurity site. Apparently the Pd $4d$ and Cu $3d$ levels more or less coincide, which is not unreasonable considering the large electronegativity of Pd, so that both the bonding and antibonding states have about equal intensity at the impurity site and at the neighboring sites. Thus we have here a situation where the large $4d$-$3d$ hybridization nearly splits off two levels at the upper and lower band edge.
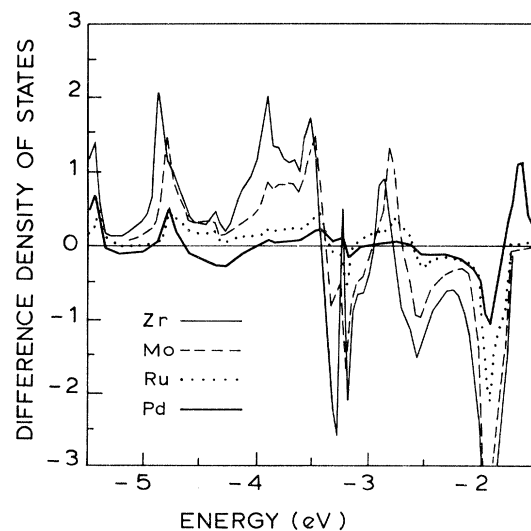

FIG. 5. Difference LDOS in Cu-neighbor Wigner-Seitz cell of some elements from the $4d$ series.

Now we want to compare our calculations for chemically equivalent 4d and 3d impurities. Figure 6 shows the LDOS for Ni and Pd impurities, both in the impurity cell and in a neighboring cell. In the Ni cell we have much less intensity within the d-band region, indicating the smaller hybridization between the Cu 3d band and the Ni 3d electrons, which are more localized than the Pd 4d electrons. Moreover, the Pd virtual bound state is appreciably lower than the Ni state, indicating the larger electronegativity of Pd. On the neighboring site the shift to lower energies is for both reasons larger for Pd. For the elements Sc and Y at the beginning of the 3d and 4d series, Fig. 7 shows the LDOS at the neighboring site and also the change of the LDOS (lower curve) with respect to the host density of states. In addition, here one sees the effect of the stronger hybridization of the 4d electrons due to their larger overlap.

Finally, we want to stress the magnitude of the change of the LDOS on the neighboring site. For instance, from Fig. 7 we see that for Sc or Y, about 2 electrons are effec-
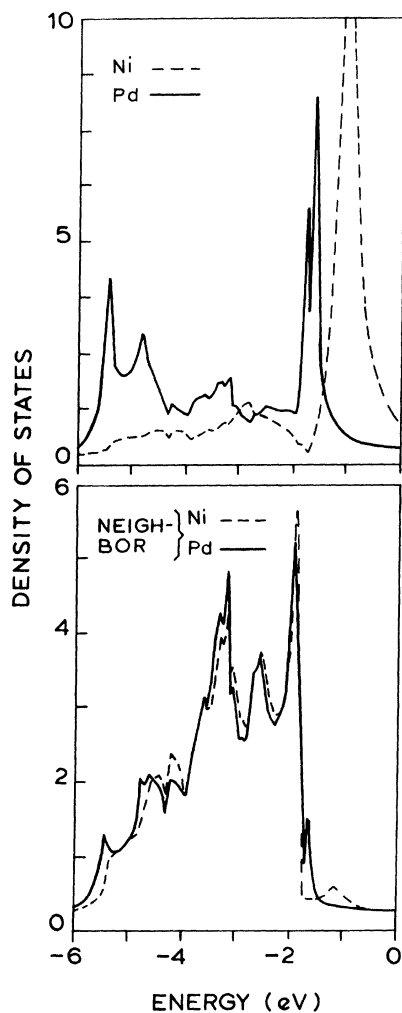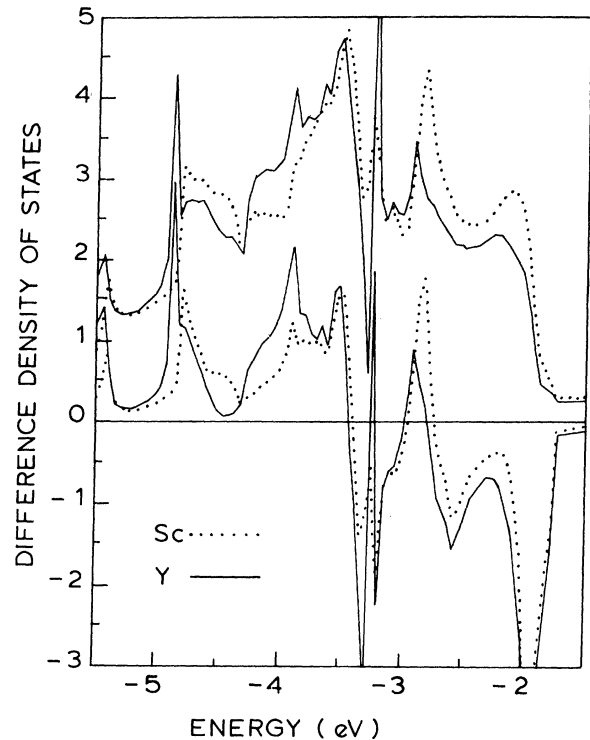

FIG. 7. LDOS (upper curves) and difference LDOS (lower curves) in the Cu-neighbor Wigner-Seitz cell of elements at the beginning of the 3d and 4d series.

FIG. 6. LDOS in the impurity Wigner-Seitz cell and Cu-neighbor Wigner-Seitz cell of elements from the end of the 3d and 4d series.

tively shifted from the upper to the lower band region, say from about −2.5 to −4.5 eV on the average. Since we must multiply this by 12 in order to obtain the change of the LDOS in the first shell, we see that this gives an enormous contribution to the change of the total density of states, which is much larger than that arising from the impurity cell. Note, however, that these relatively large and important changes of the density of states on the neighboring sites do not lead to similar large changes of the charge density or of the potential. For instance, by integrating the change of the LDOS on the neighboring site of Sc or Y, the positive and negative contributions cancel each other to a very large extent, leaving only a rather small surplus charge of 0.07 or 0.09 electron on the neighboring site (see Tables I and II).

For more distant neighbors we expect essentially the same behavior. The change of the LDOS should acquire even more oscillations; by integrating over the energy, the cancellation is even more complete so that the perturbed charge density and the perturbed potential are well localized. This is essentially why the Green's-function method is superior to cluster calculations. In the Green's-function method, the infinite spatial extent of the changed densities of states is described correctly; only the perturbed potential is assumed to be localized. Therefore in most cases a calculation with a single perturbed potential for the impurity already gives a reasonable description of the physics. In contrast, in cluster calculations rather large clusters of more than 40−50 atoms must be treated in order to

detect typical impurity properties (see the discussion in the next section).

There is practically no experimental information from x-ray photoelectron spectroscopy (XPS) measurements on the rather large changes of the density of states within the Cu d band. The only exception known to us is the work of Hüfner et al.,[39] who measured XPS difference spectra for Pd in Cu, Ag, and Au. They found a nonuniform change within the d-band region: a strong loss of intensity in the upper band region and an increase in the lower region, in agreement with the general trend we obtain. Note, however, that the calculated changes for Pd (see Fig. 5) are rather small compared to the changes, e.g., for Mo or Zr at the beginning of the $4d$ series, so that an experimental measurement of these larger changes would be quite interesting.

B. Charges in the impurity and neighboring cells; Friedel sums

In Table I the most important numerical results for the $4d$ impurities are summarized, whereas Table II gives the results for the $3d$ impurities (including the magnetic impurities). A comparison of the results for the $4d$ impurities with the single-site calculation of Braspenning et al.[13] shows that the local charges in the impurity Wigner-Seitz sphere have considerably been reduced, e.g., for Mo with a valence of 6 the local charge is 4.90 instead of 5.65 in the simpler previous calculation; for Pd it is 9.59 instead of 9.88. Apparently, the self-consistency of the single site underestimates the charge transfer and has a tendency to make the impurity cell more neutral. The charge transfer towards the Cu neighbors decreases continuously through the $4d$ series, which is partly due to the decreasing extent of the $4d$ wave functions. The same tendencies are also seen for the nonmagnetic (as well as the magnetic) $3d$ impurities for which the single-site results are given in Ref. 12. Here, however, the charge transfer is considerably smaller due to the smaller extent of the $3d$ wave functions. For the $4d$ impurities, the additional charge on the neighboring site has mostly s and p character with only a small

positive d component. Contrary to the $3d$ impurities, a sizable but negative d component exists. From the magnitude of the charge transfer it is evident that a correct treatment of the nearest neighbors is more important for the $4d$ impurities than for the $3d$ impurities.

From Table I one also sees that the cluster consisting of the impurity and the first neighbors is practically neutral, with maximal charge deviations of 0.12 for Y and -0.08 for Mo and Tc. This is even more evident for the $3d$ impurities. However, one should keep in mind that self-consistency might make the cluster more neutral than it actually is, so that the deviations might be somewhat larger.

Table I also gives the total charges calculated from the Lloyd formula, i.e., $N_{tot} = \Delta N(E_F) + N_{Cu}$. For an exact calculation the Friedel sum rule $\Delta N(E_F) = \Delta Z$ or $N_{tot} = Z_{imp}$ should be valid. Compared to the single-site calculation (SSC) this sum rule is now much better satisfied. For instance, for Y at the beginning of the series ($Z_{imp} = 3$) we obtain $N_{tot} = 3.05$ instead of the previous value 1.75, whereas for Pd at the end of the series ($Z_{imp} = 10$) we have now 10.02 instead of 10.11. This clearly shows the improvement of the present cluster calculation compared to the SSC. For the $3d$ impurities the Friedel sum rule is just as well satisfied, so that the inclusion of more neighbors should be not important.

Table I also lists the decomposition of the total charge N_{tot} into the "free-electron" part

$$N_{tot}^{free} = N_{Cu} + \frac{2}{\pi} \sum_{l,n} (2l+1) \Delta \delta_l^n (E_F) ,$$

arising from the first term in Eq. (1) due to the changed phase shifts, and the backscattering part N_{tot}^{back} due to the second term in (1) describing the multiple scattering. For both the $4d$ and $3d$ impurities N_{tot}^{free} is, in general, larger than N_{tot} or Z_{imp}. The negative backscattering decreases through the $4d$ series and is even slightly positive for Pd. Since N_{tot}^{free} is dominated by the change of the impurity phase shifts $\Delta \delta_l^{imp}$, $N_{tot}^{free} > Z_{imp}$ means that the virtual bound state for the solution of a single muffin tin in jelli-

TABLE I. Theoretical results for $4d$ impurities. The local valence charge N_{loc}^{imp} within the impurity Wigner-Seitz sphere and the deviation ΔN_{loc}^{nb} of the local charge N_{loc}^{nb} of a neighboring Cu atom from the value N_{loc}^{host} of a bulk Cu atom. The charge neutrality lists the excess or deficit charge in the cluster containing the impurity and its 12 nearest neighbors. Furthermore, the total charge $N_{tot} = Z_{host} + \Delta N(E_F)$, as calculated from the Friedel sum $\Delta N(E_F)$, is given together with its decomposition into N_{tot}^{free} and N_{tot}^{back}.

	Z_{imp}	N_{loc}^{imp}	ΔN_{loc}^{nb}	Charge neutrality	N_{tot}	N_{tot}^{free}	N_{tot}^{back}
Y	3	2.02	0.09	0.12	3.05	4.46	-1.41
Zr	4	2.79	0.10	0.01	4.02	6.08	-2.05
Nb	5	3.79	0.10	-0.05	5.01	7.28	-2.27
Mo	6	4.90	0.09	-0.08	6.01	7.96	-1.95
Tc	7	6.05	0.07	-0.08	7.00	8.40	-1.39
Ru	8	7.28	0.06	-0.06	7.99	8.75	-0.75
Rh	9	8.46	0.04	-0.03	9.00	9.23	-0.24
Pd	10	9.59	0.03	0.00	10.02	9.99	0.03

TABLE II. Theoretical results for $3d$ impurities. The same notation as in Table I is used. In addition, the corresponding magnetic quantities are given: the total moment M_{loc}^{imp} in the impurity Wigner-Seitz cell, the induced moment M_{loc}^{nb} on a neighboring Cu atom, the total momentum M_{cl} of the cluster containing the impurity and its 12 neighbors, and the total moment M_{tot} as calculated by the Friedel sum rule.

	Z_{imp}	N_{loc}^{imp}	ΔN_{loc}^{nb}	Charge neutrality	N_{tot}	N_{loc}^{free}	N_{tot}^{back}	M_{loc}^{imp}	M_{loc}^{nb}	M_{cl}	M_{tot}
Sc	3	2.22	0.07	−0.01	3.00	4.16	−1.16	0	0	0	0
Ti	4	3.21	0.06	−0.07	4.00	6.03	−2.02	0	0	0	0
V	5	4.33	0.05	−0.08	5.00	6.81	−1.81	1.28	0.02	1.47	1.47
Cr	6	5.51	0.04	−0.05	5.97	6.65	−0.68	3.09	0.03	3.39	3.36
Mn	7	6.56	0.03	−0.05	6.99	7.86	−0.87	3.44	0.02	3.65	3.59
Fe	8	7.70	0.02	−0.05	8.00	9.05	−1.05	2.55	0.01	2.62	2.55
Co	9	8.87	0.01	−0.05	8.98	9.36	−0.38	0.96	−0.00	0.95	0.92
Co[a]	9	8.89	0.01	−0.05	8.98	9.27	−0.29	0	0	0	0
Ni	10	9.98	−0.00	−0.03	9.98	9.97	0.01	0	0	0	0

[a] Result of paramagnetic calculation.

um, given by the first term in Eq. (1) and, e.g., shown in Fig. 2(a) for Mo (dashed curve), contains too many electrons. The bonding-antibonding hybridization, the effects of which are described by the backscattering term, corrects this and leads then approximately to the correct Friedel sum rule.

We have also performed calculations using different cutoff energies E_c for the host Green's function in order to study the sensitivity of the results to the cutoff approximation (5). For all $3d$ and $4d$ impurities we find that the local charges of the impurities and the first neighbors are quite insensitive to the cutoff energy E_c, with typical changes of 0.01 electron if E_c is varied from a rather low value of 3 to 16 eV above E_F. Thus apparently the local self-consistency reduces, to a large extent, errors of the Green's functions introduced by the cutoff procedure. In contrast the Friedel sums are more affected. For Mo, for instance, N_{tot} changes from 6.15 for $E_c = 3$ eV to 6.01 for $E_c = 16$ eV. All results given in Tables I, II, and III refer to a cutoff energy of 16 eV above E_F.

IV. MAGNETIC $3d$ IMPURITIES

Impurities from the middle of the $3d$ series are magnetic in simple or noble metals, since by spin alignment the electrons gain exchange energy. The occurrence of local moments is usually discussed in the Anderson model[40] or equivalently in the Wolff model,[41] which are based on Friedel's virtual-bound-state concept. Ionic aspects are stressed in the model proposed by Schrieffer[42] and Hirst.[43] We have recently performed realistic ab initio calculations for $3d$ impurities in Cu and Ag (Refs. 11 and 12) that are based on the single-perturbed-potential model. Although our results were in qualitative agreement with the Anderson model, nevertheless important qualitative differences arose due to the hybridization of the impurity d electrons with the Cu d band, which is not contained in the Anderson model. The results are, however, in strong disagreement with cluster calculations of Johnson et al.,[44] which we have criticized.[12] We come back to this point in connection with some recent cluster calculations for CuFe

and PdFe of Delley et al.[45] and Rodriquez and Keller.[46] We have also performed similar calculations for $3d$ impurities in Mo and Nb (Ref. 15) and for $3d$ impurities in Al (Ref. 14). Even in the simple metal Al, band-structure effects turned out to be important.

In order to check the reliability of our previous calculation based on the single perturbed potential and in order to obtain more reliable information about the host polarization, we have therefore recalculated the electronic structure of magnetic $3d$ impurities in Cu by also allowing perturbed potentials at the neighboring sites. Figure 8 shows the LDOS of the impurities V, Cr, Mn, and Fe in Cu for the majority and minority spins. Comparison with the results of the SSC of Zeller et al.[11] and Podloucky et al.[12] reveals only minor differences, and all qualitative aspects are the same. Especially one also sees that for the magnetic impurities the hybridization of the impurity d electrons with the host d electrons is quite important, leading for both spin directions to a division of the intensity into a smaller, bonding-type fraction within the d band and a larger antibonding type virtual bound state at higher energies. Note the hybridization minimum at the upper edge of the Cu d band. For Mn and Fe the very sharp majority virtual bound state is shifted towards the upper edge of the d band, leading to an especially large intensity within the d-band region. For the LDOS of the neighboring sites, similar but far less pronounced features as those for the $4d$ impurities or for Sc (see Figs. 4, 5, and 7) are found. The differences between the neighboring LDOS of the two spin directions are minor.

Table II summarizes the most important quantitative results for the $3d$ impurities. As with the $4d$ impurities, the local charges in the impurity cell are appreciably smaller than those in the SSC, i.e., the single-site self-consistency underestimates the charge transfer by about a factor of 2. For instance, for Mn with $Z_{imp} = 7$ the local charge is 6.56 instead of 6.79 in the SSC. Our present calculation yields V, Cr, Mn, and Fe as well as Co to be magnetic. Compared to the SSC the local moments for V and Cr are somewhat reduced, while those for Mn and Fe are slightly increased (see Fig. 9). A major discrepancy is seen
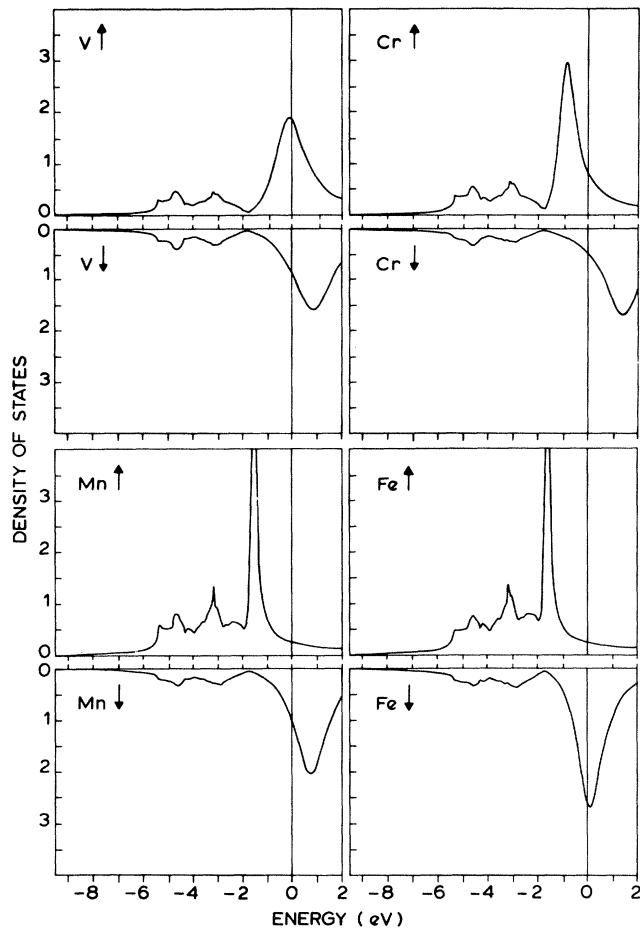
FIG. 8. LDOS in the impurity Wigner-Seitz cell for majority ($\uparrow$) and minority ($\downarrow$) spin of some $3d$ impurities in Cu.

$-0.001\mu_B$ for the fourth neighbor. These calculations also explain the very small moment at the neighboring sites of Fe and Co: When progressing in the $3d$ series, the first zero of the magnetization oscillations shifts systematically to smaller radii, so that for Co, and nearly so for Fe, the positive and negative contributions to the polarization cancel each other in the first neighboring cell.

Figure 9 shows a comparison of the calculated moments with the available experimental results for Cr, Mn, and Fe (mostly susceptibility or neutron scattering results). The present values agree somewhat better with the experimental results than the SSC. Note the appreciable scattering of the experimental data for the same material.

Whereas Ni in Cu is generally agreed to be nonmagnetic, the experimental situation is not so clear for Co, V, or Ti impurities. For a discussion of this point see, e.g., Ref. 48. Kramer and Bergmann[49] have recently found by anomalous Hall-effect measurements that Co impurities in disordered Cu films are nonmagnetic, whereas Co impurities in Ag films are magnetic. While this is in disagreement with our present result for Co in Cu, it nevertheless agrees with our general findings in Ref. 12 that the tendency for magnetism is larger in Ag than in Cu.

The experimental information about virtual bound states of magnetic impurities is somewhat conflicting. For a detailed discussion we refer to Refs. 12 and 50. Whereas Höchst et al.[51] have not been able to detect virtual bound states for magnetic impurities such as AgMn, AuFe, or CuFe, Reehal and Andrews[50] and Andrews and Brown[52] found evidence for virtual bound states for Fe and Cr in Au. For $Ag_{0.8}Mn_{0.2}$ a majority peak is identi-
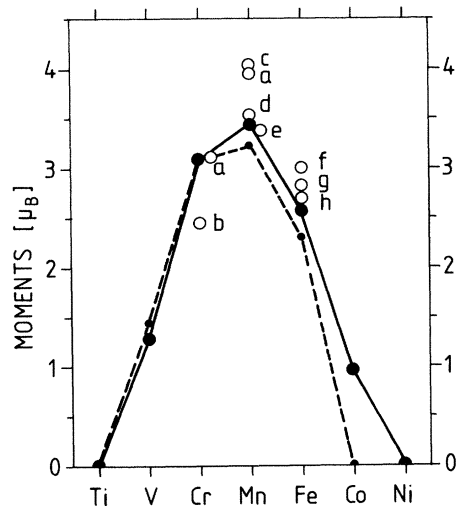
only for Co. In the SSC Co was nonmagnetic, but just on the verge of becoming magnetic as one could conclude from the extremely slow convergence of the self- consistency iterations. In the present ICC we obtain a moment of $0.96\mu_B$ for Co. This rather large change is not too surprising since near the threshold a rather small change of physical quantities may result in a large change for the moment. Overall, however, our present elaborate calculations confirm the simpler SSC values quite well, as can be seen from Fig. 9.

The neighboring atoms become slightly ferromagnetic-polarized, with the largest moment of $0.025\mu_B$ for a Cr neighbor, $0.017\mu_B$ for a Mn neighbor, and $0.006\mu_B$ for a Fe neighbor. Practically the same values for the polarization of the first neighbors have been recently obtained by Deutz[47] for the single-site model, so that the Cu-host magnetization, contrary to the charge transfer, seems to be well described in the single-site model. Moreover, the moment of the cluster agrees quite well with the total moment, so that the polarization of the more distant neighbors is not important. For instance, Deutz obtains for Mn in the single-site model $0.016\mu_B$ for the first neighbor, $-0.006\mu_B$ for the second, $0.000\mu_B$ for the third, and

FIG. 9. Local moments in the impurity Wigner-Seitz cell for $3d$ impurities in Cu. ●, present calculations; ·, SSC; ○, experimental values. a, W. D. Weiss, Z. Metallk. 58, 909 (1967); b, M. Vochten, M. Labro, and S. Vynckier, Physica 86-88B, 467 (1977); c, C. M. Hurd, J. Phys. Chem. Solids 30, 539 (1969); d, J. R. Davies and T. J. Hicks, J. Phys. F 9, 753 (1979); e, Ref. 56; f, J. R. Davies and T. J. Hicks, J. Phys. F 9, L7 (1979); g, P. Steiner, S. Hüfner, and W. V. Zdrojewsky, Phys. Rev. B 10, 4704 (1974).

fied at -2.8 eV below E_F in agreement with earlier findings of Norris and Wallden[53] and Wallden.[54] Cohen and Slichter[48] have recently performed jellium-type calculations for $3d$ impurities in Cu and have fitted their results to NMR satellite data for these impurities. The resulting positions of the virtual bound states for Fe, Mn, and Cr are in astonishing agreement with our *ab initio* calculations except for the majority peaks of Fe and Mn for which band-structure effects, not included in a jellium calculation, are very important.

Coleridge *et al.*[52] have performed de Haas—van Alphen measurements at very dilute CuCr, CuMn, and CuFe. Their results are in qualitative agreement with the location of the virtual bound states found in our calculations, i.e., resonance scattering at the minority virtual bound state for Fe, a strongly asymmetrical scattering for both spin directions for Mn, and no additional magnetic scattering for Cr due to the more or less equal densities of states for both spin directions at E_F. Recently Higgins and Hendel[53] made a detailed dHvA study for CuMn. From their measurements they infer a moment of $3.4\mu_B$ (our value 3.44). Moreover, their measured ratio of the spin-up—spin-down scattering of 0.25 favorably agrees with our values for the corresponding local densities of states at E_F [$n^+(E_F)/n^-(E_F) \cong 0.27$].

Our present and previous results are strongly conflicting with the cluster calculations of Johnson *et al.*,[44] who obtained an extremely small exchange splitting for the virtual bound states of CuFe and CuMn. In contrast, Delley *et al.*[45] recently performed cluster calculations for AgFe and for PdFe. By paying special attention to the local properties of the impurities, they obtain for Fe in Ag a local moment of $2.9\mu_B$, in satisfactory agreement with our SSC (Refs. 11 and 12), yielding $2.94\mu_B$. The resulting exchange splitting of the Fe virtual bound states (1.7 eV) is somewhat smaller than our value (2.2 eV) but still an order of magnitude larger than that of Johnson *et al.* For Fe in Pd Delley *et al.* obtain agreement with recent cluster calculations of Rodriquez and Keller.[46] The calculated iron moments are $3.2\mu_B$ and $3.3\mu_B$. For the same system an unpublished SSC result by one of us (R.Z.) gives $3.4\mu_B$.

V. SOME sp IMPURITIES: VACANCY, H, He, Mg, Si, AND Ag IN Cu

In this section we present results for some selected sp impurities in Cu, e.g., for Mg and Si as well as for Ag.

Furthermore, we treat substitutional H and He, i.e., H and He trapped in a Cu vacancy. The results for the vacancy itself have already been published[23]; a preliminary account has been presented in a conference proceedings.[57]

Figure 10 gives the LDOS for the substitutional impurities H and He and for the vacancy for which both the cluster result and the SSC result are given. For the vacancy we find a strong s peak at -4.2 eV and a smaller peak of s and p character at -3.2 eV. From this strong structure it is clear that the hybridization with the Cu d band is quite important. It is of interest to point out the close similarity of the LDOS for the vacancy with that for a Na impurity.[13] Even minor features of the density of states are similar, and in both cases roughly one electron is attracted by the impurity cell (see Table III). For H we obtain a very broad s intensity below the d band. This is quite contrary to interstitial hydrogen for which usually a bound state just below the band minimum, say at about -10 eV, is obtained. The difference is due to the weaker electrostatic potential of the host atoms that the hydrogen "feels" at the substitutional site. For He a bound $1s$ state below the band minimum is found, which is not shown in Fig. 10.

Figure 11 shows the difference LDOS (neighbor LDOS minus the host LDOS) at the perturbed neighbor sites of H, He, and the vacancy, while again the SSC results for the vacancy are added. In all three cases quantitatively similar results are obtained. States are removed from the lower-d band region and are added at higher energies. This is just the opposite trend as found for the $4d$ and $3d$ impurities, shown in Figs. 5 and 7. One could be tempted to describe this by the simple bonding and antibonding model of Fig. 3. Since the local energy levels of H and He are lower than the Cu $3d$ levels the bonding levels are now more localized on the impurity site, while the higher antibonding levels are more localized on the neighboring sites. However, at least for He this explanation has some problems, since the overlap between the He $1s$ states and the Cu $3d$ states is exceedingly small (see below).

Figure 12 shows the spherically averaged charge density for the vacancy and for H and He trapped in the vacancy. In the vacancy Wigner-Seitz cell a local charge of 1.07 electrons is found, which is considerably larger than the SSC number of 0.67 electron. Since the cluster consisting of the vacancy and the 12 nearest neighbors is practically neutral, there is a considerable charge transfer from the

TABLE III. Theoretical results for some sp impurities (same notation as in Table I).

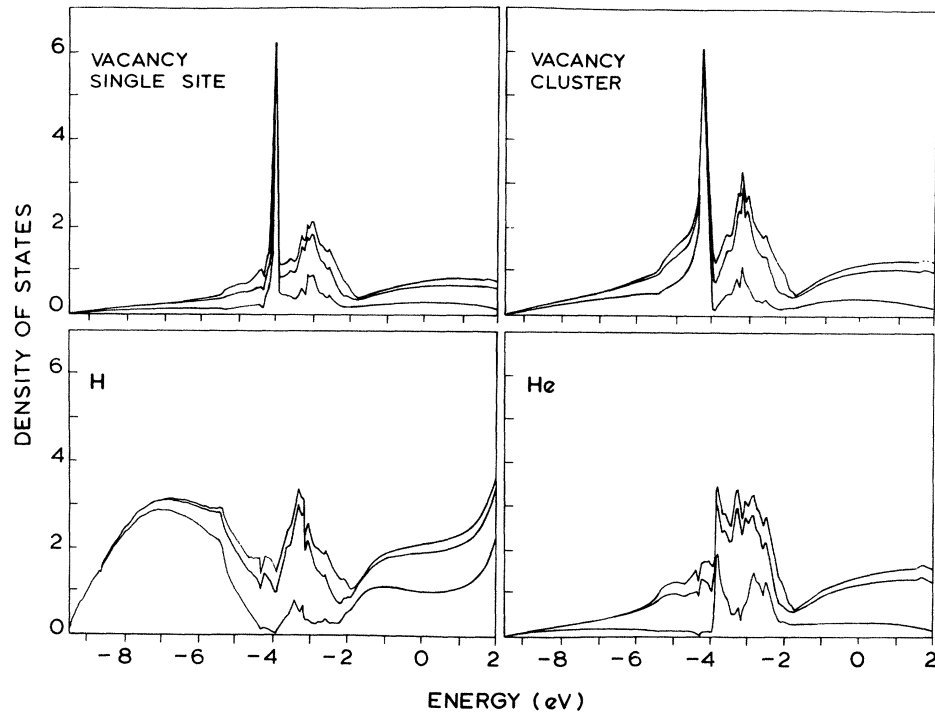|	Z_{imp}	N_{loc}^{imp}	ΔN_{loc}^{nb}	Charge neutrality	N_{tot}	N_{tot}^{free}	N_{tot}^{back}
Vacancy	0	1.07	-0.08	0.06	$+0.02$	-0.30	0.32
H	1	2.05	-0.08	0.11	1.05	1.07	-0.02
He	2	2.94	-0.07	0.05	1.95	1.56	0.38
Mg	2	1.64	0.03	0.00	1.99	2.17	-0.18
Si	4	3.60	0.04	0.04	3.97	4.70	-0.73
Ag	11	10.53	0.04	0.03	11.04	11.06	-0.03

FIG. 10. LDOS of the vacancy and of substitutional H and He impurities. The bound state of He is not shown. For the vacancy both the single-site result and the present "cluster" result are given.
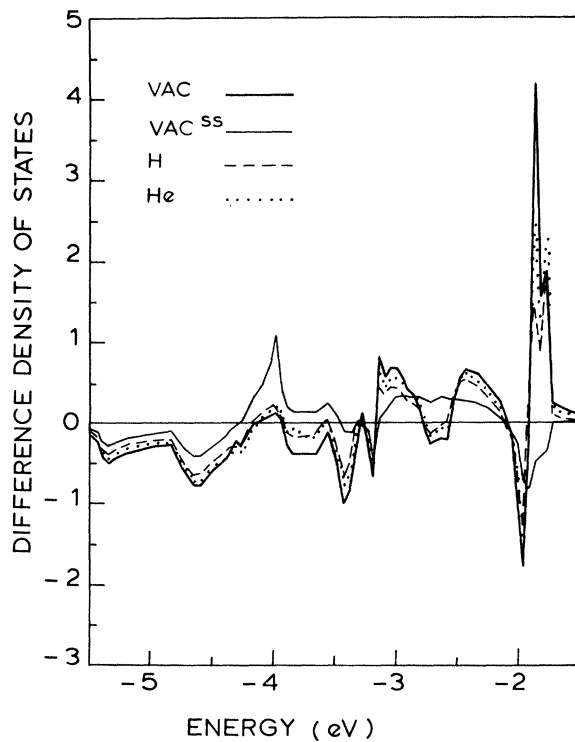
first neighbors into the vacancy (see Table III). The charge density at the center of the vacancy is 0.5 electron per atomic cell, being about a factor of 4 smaller than the density at the Wigner-Seitz radius. For He the charge density is strongly concentrated in the center of the cell, while it follows the charge-density behavior of the vacancy in the neighborhood of the Wigner-Seitz boundary. Thus apparently the atomic He density simply superimposes the density in the vacancy. This is, however, not quite true: The total charge in the impurity cell is 2.94 in-

FIG. 11. Difference LDOS in the Cu-neighbor cell of the vacancy and of substitutional H and He.
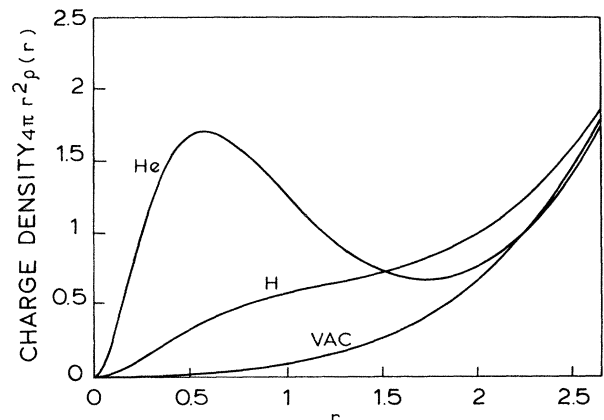
FIG. 12. Spherically averaged charge density (a.u.) in the Wigner-Seitz cell of the vacancy and of substitutional H and He.

stead of $1.07 + 2 = 3.07$ if the superposition would hold. The difference is also clear: The full $1s$ core of He acts as a weak and repulsive pseudopotential that diminishes the density in the center of the vacancy cell. However, at the boundary and at the neighboring sites the vacancy properties are more or less unperturbed, which explains the close agreement between the LDOS on the neighboring sites for He and the vacancy. Compared to He, substitutional H seems to be an intermediate case. While fairly localized, there seems to be enough overlap with the Cu d electrons in order to make the above bonding-antibonding discussion meaningful.

Similar to the case of the vacancy, the SSC results for substitutional H and He are unreliable. For instance, for He no bound $1s$ state is obtained. A large part of this discrepancy seems, however, to be connected with the determination of the perturbed single-site potential in the single-site calculation. For this we have only taken the perturbed charge density *within* the perturbed muffin-tin into account, thus completely neglecting the perturbed charge outside. In contrast, Terakura *et al.*[8] and Katajama-Yoshida *et al.*[9] and also Klein and Pickett[20] take the perturbed charge outside into account by reasonably extrapolating the single-site solution beyond the muffin-tin radius. As has recently been demonstrated by Klein and Pickett[58] for the vacancy in Al, this can considerably improve the quality of the single-site solution, especially in cases where the charge transfer is very important. Note that in the present cluster calculation this problem does not arise since the charge density within the impurity site and the first neighbor sites is treated exactly.

Figure 13 shows the LDOS for the sp impurities Mg and Si together with Ag. The density of states is decomposed into s, $s + p$, and $s + p + d$ contributions. The results are very similar to the SSC.[13] The main characteristics for Mg and Si are bonding and antibonding peaks below and above the d band, while for Ag a virtual bound state below the d band appears. Figure 14 shows the difference LDOS for the neighbors of Mg, Si, and Ag. Again a large repopulation is seen within the d band. Especially for Mg and Si we have a strong shift of the intensity from higher to lower energies, while for Ag the sit-

uation is more complex. In all cases intensity is lost at the upper band edge. From Table III one sees that for Mg and Si there is an appreciable charge transfer from the impurity to the neighbors: 0.36 and 0.40 electrons, respectively, are missing in the impurity cell.

The total charges calculated using the Friedel sum are in good agreement with the valence of the impurity (Z_{imp}). The improvement compared to the single-site calculations is quite remarkable. For instance, for Mg $(Z_{imp} = 2)$ the Friedel sum gives 1.99 instead of 1.52 in the SSC, whereas for the vacancy $(Z_{imp} = 0)$ we obtain now 0.02 instead of 0.25 previously. Clearly, longer-ranged potential perturbations are not important.

The present calculation refers to a cutoff energy for $\tilde{G}$ of $E_c = 16$ eV above E_F. The results are quite stable with respect to variations of E_c. For instance, even if a rather low cutoff energy of $E_c = 3$ eV is chosen as in Ref. 23, the local charge in the vacancy changes only from 1.07 to 1.10 electrons, whereas somewhat larger changes are obtained for the Friedel sum N_{tot} (-0.05 instead of $+0.02$).

VI. SUMMARY AND CONCLUSIONS

The calculations presented in this paper show that the KKR Green's-function method is capable of including potential perturbations both at the impurity site and at the neighboring host sites. In this sense the present calculations are a natural extension of the previous single-site calculations.[13] Our calculations demonstrate that very often a single perturbed potential gives a good qualitative description of the defect properties and that the addition of one shell of perturbed host potentials gives good quantitative results. This indicates the advantage of the present approach compared to conventional cluster calculations. Only the perturbed potentials enter as a perturbation in the Dyson equation. Since they are strongly localized, the corresponding clusters to be considered can be quite small, so that often only a single perturbed potential is sufficient.

Our study shows that the influence of the Cu neighbors on the $3d$ impurities is rather small; it is larger for the $4d$ impurities. The LDOS of the impurity consists of the vir-
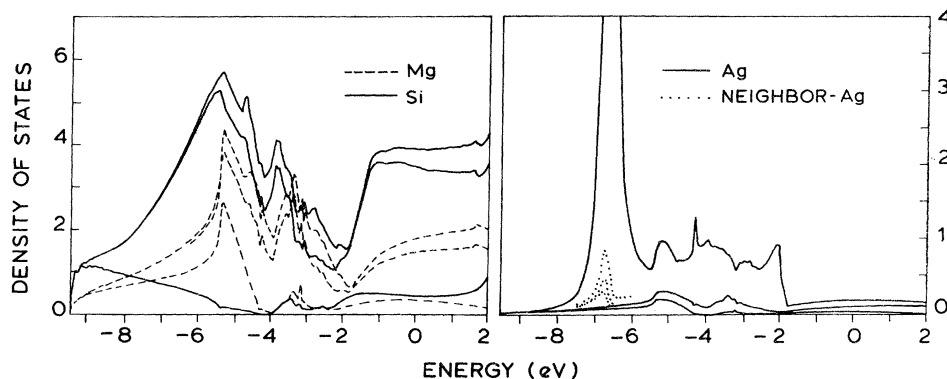

FIG. 13. LDOS in the impurity Wigner-Seitz cell of Mg, Si, and Ag. The influence of the Ag virtual bound state on the LDOS of a Cu neighbor is also shown (dotted).
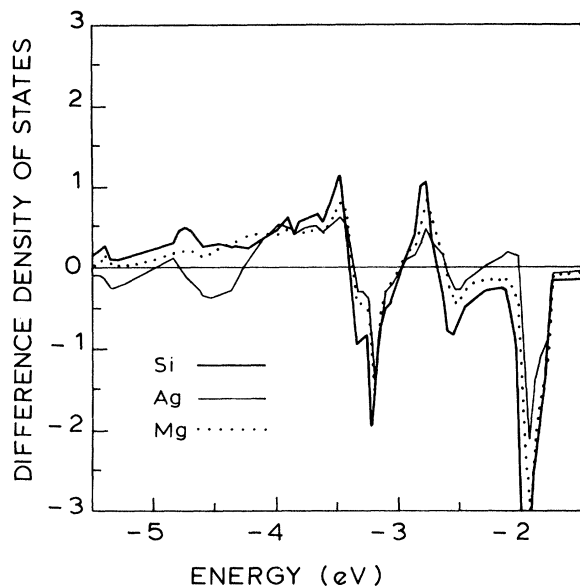
FIG. 14. Difference LDOS in the Cu neighbor Wigner-Seitz cell of Mg, Si, and Ag.

tual bound state, which is mostly strongly asymmetrical, and of an appreciable intensity within the Cu d band. These structures can be understood as the antibonding and bonding combinations of the impurity d orbitals with the host d electrons. While the changes of the charge density and the potential on the neighboring sites are rather small, the LDOS of the neighbors shows an important shift of the intensity from the higher part of the d band to the lower part, especially for $4d$ impurities. We therefore predict such an effect in future XPS difference spectra.

Our calculations for the magnetic $3d$ impurities essentially confirm the previous results based on a single perturbed potential. The calculated moments for Cr, Mn, and Fe in Cu are somewhat larger than those in the SSC and in general are in somewhat better agreement with the experimental data. The neighboring host atoms become slightly polarized, and the polarization of more distant atoms seems to be very small. In contrast to the SSC, Co in Cu is obtained as magnetic with a local moment of $0.96\mu_B$. This is, however, a very critical case since in the SSC Co was just on the verge of becoming magnetic.

For the vacancy in Cu and for substitutional H and He impurities the inclusion of perturbed potentials at the neighboring sites is quite important. Locally, we obtain 1.07 electrons in the vacancy cell and 2.05 and 2.94 electrons, respectively, in the impurity cell for H and He. Thus there is a considerable charge transfer into the impurity cell, contrary to the SSC results.

We are convinced that the experience gained with the present calculation allows for considerable improvement in the future. For instance, more shells of perturbed potentials can be included, so that a realistic calculation of Friedel oscillations in the first shells around the impurity is feasible. Lattice relaxations could be included along the lines suggested by Lodder.[59] More complicated defects, e.g., impurity pairs with perturbed neighboring potentials, can be treated, etc. In all cases the computer time needed does not seem to be prohibitive due to the combined use of improved iteration schemes, complex-energy integration, and group theory

ACKNOWLEDGMENTS

[1]G. F. Koster and J. C. Slater, Phys. Rev. **95**, 1167 (1954).
[2]G. A. Baraff and M. Schlüter, Phys. Rev. Lett. **41**, 892 (1978).
[3]G. A. Baraff and M. Schlüter, Phys. Rev. B **19**, 4965 (1979).
[4]J. Bernholc, N. O. Lipari, and S. T. Pantelides, Phys. Rev. Lett. **41**, 895 (1978).
[5]J. Bernholc, N. O. Lipari, and S. T. Pantelides, Phys. Rev. B **21**, 3545 (1980).
[6]T. H. Dupree, Ann. Phys. (N.Y.) **15**, 63 (1961).
[7]J. L. Beeby, Proc. R. Soc. London Ser. A **302**, 113 (1967).
[8]K. Terakura, J. Phys. Soc. Jpn. **40**, 450 (1976); J. Phys. F **6**, 1385 (1976); Physica **91B**, 162 (1977).
[9]H. Katajama-Yoshida, K. Terakura, and J. Kanamori, J. Phys. Soc. Jpn. **46**, 822 (1979); **48**, 1504 (1980); **49**, 973 (1980).
[10]R. Zeller and P. H. Dederichs, Phys. Rev. Lett. **42**, 1713 (1979).

[11]R. Zeller, R. Podloucky, and P. H. Dederichs, Z. Phys. B **38**, 165 (1980).
[12]R. Podloucky, R. Zeller, and P. H. Dederichs, Phys. Rev. B **22**, 5777 (1980).
[13]P. J. Braspenning, R. Zeller, P. H. Dederichs, and A. Lodder, J. Phys. F **12**, 105 (1982).
[14]J. Deutz, P. H. Dederichs, and R. Zeller, J. Phys. F **11**, 1787 (1981).
[15]R. Podloucky, J. Deutz, R. Zeller, and P. H. Dederichs, Phys. Status Solidi B **112**, 515 (1982).
[16]R. Zeller, in *Physics of Transition Metals 1980*, edited by P. Rhodes (IOP, Bristol, 1980), p. 265; R. Zeller (unpublished).
[17]C. Koenig and E. Daniel, J. Phys. (Paris) Lett. **42**, L-193 (1981).
[18]C. Koenig, P. Leonard, and E. Daniel, J. Phys. (Paris) **42**, 1015

(1981).

[19]P. Leonard and N. Stéfanou, Ann. Phys. (Paris) 43, 1497 (1982).

[20]B. M. Klein and W. E. Pickett, in *Proceedings of the International Symposium on the Electronic Structure and Properties of Hydrogen in Metals, Richmond, Virginia, 1982*, edited by P. Fena and C. B. Satterthwaite (Plenum, New York, 1983).

[21]J. E. Inglesfield, J. Phys. C 14, 3795 (1981); J. Phys. F 11, L287 (1981).

[22]R. Zeller, J. Deutz, and P. H. Dederichs, Solid State Commun. 44, 993 (1982).

[23]R. Zeller and P. J. Braspenning, Solid State Commun. 42, 701 (1982).

[24]O. Gunnarsson, O. Jepsen, and O. K. Andersen, Phys. Rev. B 27, 7144 (1983).

[25]D. B. B. Rijsenbrij and A. Lodder, J. Phys. F 6, 1053 (1976).

[26]G. Ries and H. Winter, J. Phys. F 9, 1589 (1979).

[27]C. Koenig, J. Phys. F 3, 1497 (1973).

[28]H. Dreysse and R. Riedinger, J. Phys. (Paris) 42, 437 (1982).

[29]A. R. Williams, P. J. Feibelman, and N. D. Lang, Phys. Rev. B 26, 5433 (1982).

[30]G. Lehmann, Phys. Status Solidi B 70, 737 (1975).

[31]P. Lloyd, Proc. Phys. Soc. London 90, 207 (1967).

[32]P. J. Braspenning, thesis, Vrije Universiteit Amsterdam, 1982 (unpublished).

[33]P. C. Hohenberg and W. Kohn, Phys. Rev. 136, B864 (1964); W. Kohn and L. J. Sham, *ibid.* 140, A1133 (1965).

[34]L. Hedin and B. I. Lundqvist, J. Phys. C 4, 2064 (1971).

[35]U. von Barth and L. Hedin, J. Phys. C 5, 1629 (1972).

[36]V. L. Moruzzi, J. F. Janak, and A. R. Williams, *Calculated Electronic Properties of Metals* (Pergamon, New York, 1978).

[37]P. H. Dederichs and R. Zeller, Phys. Rev. B 28, 5462 (1983).

[38]D. G. Anderson, J. Assoc. Comput. Mach. 12, 547 (1965).

[39]S. Hüfner, G. K. Wertheim, and J. H. Wernick, Solid State Commun. 17, 1585 (1975).

[40]P. W. Anderson, Phys. Rev. 124, 41 (1961).

[41]P. A. Wolff, Phys. Rev. 124, 1030 (1961).

[42]J. R. Schrieffer, J. Appl. Phys. 38, 1143 (1967).

[43]L. L. Hirst, Phys. Kondens. Mater. 11, 255 (1970); Z. Phys. 241, 9 (1971).

[44]K. H. Johnson, D. D. Vredensky, and R. P. Messmer, Phys. Rev. B 19, 1519 (1979).

[45]B. Delley, D. E. Ellis, and A. J. Freeman, Phys. Rev. B 27, 2132 (1983).

[46]A. Rodriguez and J. Keller, J. Phys. F 11, 1423 (1981).

[47]J. Deutz, thesis, Technische Hochschule Aachen, 1982, Kernforschungsanlage Jülich Report No. 1805 (unpublished).

[48]J. D. Cohen and C. P. Slichter, Phys. Rev. B 22, 45 (1980).

[49]I. Kramer and G. Bergmann, Z. Phys. B 47, 321 (1982).

[50]H. S. Reehal and P. T. Andrews, J. Phys. F 10, 1631 (1980).

[51]H. Höchst, P. Steiner, and S. Hüfner, Z. Phys. B 38, 201 (1980).

[52]P. T. Andrews and L. T. Brown, in *Physics of Transition Metals 1980*, Ref. 16, p. 141.

[53]C. Norris and L. Wallden, Solid State Commun. 7, 99 (1969).

[54]L. Wallden, Philos. Mag. 21, 571 (1970).

[55]P. T. Coleridge, G. B. Scott, and I. M. Templeton, Can. J. Phys. 50, 1999 (1972).

[56]R. J. Higgins and R. H. Hendel, Solid State Commun. 39, 47 (1981).

[57]R. Zeller, P. J. Braspenning, J. Deutz, R. Podloucky, and P. H. Dederichs, in *Point Defects and Defect Interactions in Metals*, edited by J. Takamura, M. Doyama, and M. Kiritani (University of Tokyo Press, Tokyo, 1982).

[58]B. M. Klein and W. E. Pickett (private communication).

[59]A. Lodder, J. Phys. F 6, 1885 (1976).